Received: 13 May 2021 | Revised: 30 June 2021 | Accepted: 25 July 2021

DOI: 10.1111/iwj.13665

ORIGINAL ARTICLE

IWJ WILEY

Novel fabrication of antibiotic containing multifunctional silk fibroin injectable hydrogel dressing to enhance bactericidal action and wound healing efficiency on burn wound: In vitro and in vivo evaluations

Meiping Dong[1] | **Yi Mao**[1] | **Zhiwei Zhao**[1] | **Jinbo Zhang**[2] | **Lipeng Zhu**[2] | **Linlu Chen**[2] | **Liexiang Cao**[1]

[1]Emergency Center, The First People's Hospital of Wenling, Wenling, China

[2]Department of Burns, The First People's Hospital of Wenling, Wenling, China

Correspondence
Liexiang Cao and Linlu Chen, The First People's Hospital of Wenling,
No. 333, Chuanan South Road, Chengxi street, Wenling 317500, China.
Email: liexiangcao@hotmail.com, chen.linlu@yahoo.com

Abstract

The development of biologically active multifunctional hydrogel wound dressings can assist effectively to wound regeneration and also has influenced multiple functions on wound injury. Herein, we designed a carbon-based composited injectable silk fibroin hydrogel as multifunctional wound dressing to provide effective anti-bacterial, cell compatibility and in vivo wound closure actions. Importantly, the fabricated injectable hydrogel exhibit sustained drug delivery properties, anti-oxidant and self-healing abilities, which confirm that composition of hydrogel is highly beneficial to tissue adhesions and burn wound regeneration ability. Frequently, designed injectable hydrogel can be injected into deep and irregular burn wound sites and would provide rapid self-healing and protection from infection environment with thoroughly filled wound area. Meanwhile, incorporated carbon nanofillers improve injectable hydrogel strength and also offer high fluid uptake to hydrogel when applied on the wound sites. In vitro MTT cytotoxicity assay on human fibroblast cell lines establish outstanding cytocompatibility of the injectable hydrogel and also have capability to support cell growth and proliferations. In vivo burn wound animal model results demonstrate that the hydrogel dressings predominantly influenced enhanced wound contraction and also promoted greater collagen deposition, granulation tissue thickness and vascularization. This investigation's outcome could open a new pathway to fabricate multifunctional biopolymeric hydrogel for quicker burn wound therapy and effectively prevents microenvironment bacterial infections.

KEYWORDS
antibiotic, in vivo burn wound, injectable hydrogel, MTT assay, nanofillers

Key messages

- an antibiotic-loaded hydrogel-based biocomposite was prepared for burn wound
- evaluated the antibacterial activity against clinically approved bacterial pathogens
- in vitro cytocompatibility were performed to imply the suitability of hydrogel
- probable effect on reepithelialisation has been confirmed *by* in vivo analysis

1 | INTRODUCTION

Worldwide, more people (300 000/annum) die from burn injuries caused by fire, radiation, chemical and electrical accidents.[1,2] The burn wounds with deep-partial thickness are very difficult to heal and also have more complications in many cases, and such wound gives problems to internal organs and tissues that exist underneath human skin.[3,4] Consequently, it is highly challenging to treat burn wound injuries because it has complex healing inhibiting factors including irregular shape, injury size, bigger wound exudation and problems to find injured areas, etc. Hence, the design of wound dressing materials for burn wound therapy should be finely merited and adopted to irregularly shaped wound sites and predominantly played on the wide wound area.[5,6] The development of sterilised and moist wound dressing with antimicrobial efficacy would be more desirable for future generation burn wound treatments, which will provide quick healing with infection control treatment. Generally, wound dressing materials should be replaced in a proper interval in the burn wound therapy, when the outer body fluids soaking through it to prevent microbial infections.[7,8] Thus, simply removed and painlessly handled wound dressing would be ideal material to improve burn wound healing efficiency and decrease mortality rate. Fabrication of biocompatible hydrogel dressings may offer promising alternative for other burn wound dressing, because their supreme properties of wound exudate absorption and moist microenvironment can be favoured to sustain healing with determined protection against infections. Particularly, self-healing hydrogels signify a new generation smart dressing, which could have the ability to regenerate a collapsed network of burn wound.[9,10]

Because of the development in eco-friendly based material research to prevent synthetic hazardous materials from biological applications, naturally occurring polymers such as chitosan, cellulose, silk fibroin obtained from renewable sources are potentially applied in pharmaceutical applications.[11-13] In recent decades, hydrogel fabricated by biopolymers has great attention for various applications, particularly in biomedical applications. Because of their tailorable chemical and physical characteristics and also greater similarities to the soft skin tissues, biological hydrogels have become an innovative material for different biomedical applications such as hard tissue regeneration applications, drug delivery, biosensing and soft wound healing applications.[14-16] In addition, biological hydrogels have established more consideration in wound healing applications due to their outstanding bioactivity, biodegradability, cell compatibility and high availability.[17,18] Silk fibroin (SF), a widely available natural protein biopolymer from the source of *B. mori* cocoons, has well-established properties for biomedical applications and also has promising support to prepare biocompatible hydrogels for wound regeneration application. However, its weak mechanical strength, biodegradation and abridged gelation rate of silk fibroin are the primary limitations to be applied in biomedical area.[19-21] To overcome these physiological complications, various approaches have been used including pH, temperature control and external stimuli applications via electric techniques. Importantly, incorporation of inorganic nanomaterials, additional polymers, surfactants and functional cross-linkers can be also used to tailor its physiological properties, producing SF hydrogels with sustainable, biodegradation, drug release and mechanical strength for pharmaceutical applications.[22-24]

Prominently, many inorganic nanomaterials have been introduced into the biological SF hydrogel network to improve their wound healing efficacy along with haemostatic ability and anti-microbial actions.[25-27] In recent decades, carbon-based nanofillers were incorporated, including graphene, carbon nanotube, graphene oxide and carbon nitride, in hydrogel scaffolds, which would enhance the mechanical strength and biological functions. Particularly, modified graphene oxide

nanomaterials are auspiciously favourable and have specific attentions to the tissue regeneration and wound healing applications because of their massive hydrophobic nature, mechanical strength and high surface area.[28,29] Previous studies reported that functionalization of graphene oxide materials could improve their unique biological characteristics such as functional efficacy, cytocompatibility and water dispersibility. In particular, carboxyl and amine-modified graphene materials were found to be more biocompatible and also cryoprotective as described in reported literatures. Therefore, fabrication of multifunctional SF hydrogel incorporated with graphene oxide nanomaterials is greatly desirable for improved anti-microbial and haemorrhage management in burn wound healing treatment.[30,31]

Generally, different types of antibiotics have been widely applied for wound healing applications including gentamicin sulphate, neomycin, tobramycin, ofloxacin, chloramphenicol and bacitracin to avoid complications of microbial infections.[32-36] Ciprofloxacin is a well-known and widely used antibiotic drug for fungal and bacterial infections for wound healing treatment. Importantly, sustained delivery of anti-microbial drug molecules on infected injured wound sites is considered to be effective method with minimal side effects.[37,38] Hence, incorporation of anti-microbial drugs into the biopolymer hydrogel network can be an ideal drug delivery system for infected wound therapy. The combination of ciprofloxacin and SF hydrogel as a wound dressing material would provide protected moist environment, absorb wound exudate, autolytic debridement and infection control. In the present investigation, we have designed and fabricated GO-incorporated SF hydrogel loaded with ciprofloxacin drug, which would provide promising anti-bacterial inhibition with sustained release of drug in the burn wound treatment.

2 | EXPERIMENTAL DETAILS

2.1 | Materials

The regenerated silk fibroin (SF) solution was isolated from *B. mori* cocoons (Zhejiang Jiaxin Silk Ltd.) as previous protocols with slight modifications. Graphite flakes, lithium bromide (>99%), sodium nitrate, hydrogen peroxide and potassium permanganate were purchased from Shanghai Aladdin Chemical Technology Co. Ltd, PR China. Biological materials such as CCK-8 kit, cell culture mediums (FBS, DMEM, Trypsin–EDTA, penicillin-streptomycin) were obtained from Gibco and Life technologies, respectively. All chemicals, reagents and biological medium were used as received without further purifications.

2.2 | Preparation of regenerated SF solution

The SF regenerated solution was isolated from obtained raw *B. mori* silk material as followed in previously reported protocol with little modifications.[39,40] In brief, degumming process was performed to *B. mori* cocoons by using Na_2CO_3 under boiling distilled water for 40 minutes and washed thoroughly for three times to remove attached sericin particles. After that, dried and small pieced SF fibres were dissolved into freshly made lithium bromide (LiBr; 9.3 M) and kept in an oven at 60°C for 6 hours. The prepared colloidal SF solution was dialysed against distilled water with proper duration water change for 3 days to eradicate salts present in the SF solution. Finally, the dialysed solution was centrifuged at 9500 rpm and stored at 4°C for further uses.

2.3 | Fabrication of GO-incorporated SF hydrogel dressing

Graphene oxide was systematically prepared by using graphite powder through modified Hummer's method.[18,41] For fabrication of GO-incorporated SF hydrogel dressing, GO (3 wt%) dispersion was added into the regenerated SF solution under the sonication method, which was performed to obtain uniform distribution in the SF polymeric network. After that, the prepared mixture was constantly stirred for 20 minutes and continued sonication repeatedly three times for effective distribution of GO nanofillers. The attained GO-distributed SF mixture was centrifuged at 6000 rpm for 20 minutes to eliminate unreacted agglomerated particles. Subsequently, the appropriate amount of aqueous PEG and EDC-NHS cross-linking agent were added into the above mixture under constant stirring for 1 hour. The fabricated gel was poured into Teflon plates and dialysed against deionised water to eliminate unreacted components. The prepared hydrogel sample was labelled as GO/SF group in the presentations.

2.4 | Ciprofloxacin-loaded GO/SF hydrogel wound dressing

Primarily, ciprofloxacin solution was prepared by obtained CF (5 mg/mL) dissolving into HCl (0.1 N) and DI water and the pH of the medium was maintained between 5.0 and 5.2. To fabricate dressing materials, the prepared CF solution medium suspended to previously prepared GO/SF hydrogel network under constant stirring for 20 minutes with the addition of PEG and EDC-

NHS cross-linking agents as same as previously mentioned method. Finally, the resultant hydrogel slurry was methodically poured in a poly-TFE mould and lyophilised for 24 hours at −40°C for chemical and morphological characterizations.

2.5 | Materials characterizations

The smooth morphology and porous nature of the prepared hydrogel was microscopically observed by SEM (Phenom ProX, Netherland) and TEM (Hitachi, H-7000, Japan) techniques. The structural characterizations, phase purity, crystalline behaviour and elemental distributions of the lyophilised hydrogel groups were investigated through X-ray diffractometer (XRD; X'tra, SkinTag, USA), FTIR spectrometer (Nicolet magna IR 750; TS, USA) and XPS (XSAM-800; Kratos Co. Ltd., England) methods, respectively.

2.6 | In vitro anti-bacterial study

2.6.1 | Broth dilution assay

The bactericidal efficiency of the CF-loaded hydrogel dressings were evaluated by in vitro broth dilution assay method against clinically approved bacterial pathogens such as *S. aureus* and *E. coli* bacterial cells. Firstly, the experimental plates and devices were sterilised at 120°C for 20 minutes. After that, LB broth medium was transported to sterile Petri dish and plates kept at 4°C to obtain the solidified media. Then, selected bacterial microorganisms (10^6 CFU/mL) were systematically diffused into the solidified agar medium and incubated into shaking biological incubator at 37°C for 12 hours. The number of microbial colonies after sample incubation was analysed by using spectrophotometer at an absorbance of 600 nm as followed by previous protocols.

2.6.2 | In vitro growth curve analysis

The anti-bacterial efficacy of the prepared samples was further analysed by quantitative measurement of bacterial growth curve via standard microdilution method as followed by previous protocol. The bacterial cultured stains were prepared under LB broth medium (10 mL) in the well-plates. After that, 0 to 40 μg/mL of nanocomposite was treated with prepared bacterial strains supplemented with media and incubated in the shaking incubator at biological temperature (37°C) for 12 hours. The bacterial growth rate after different concentration of samples treatment was examined under UV–Vis spectrophotometer at optical density (OD) of 595 nm with proper time intervals. Finally, growth curves were graphed against OD versus Time.

2.6.3 | Biofilm assay

The observation of biofilm inhibition and bacterial viability after treatment of prepared hydrogel groups onto the biofilm-cultured strain was exhibited by Carl Zeiss confocal laser scanning microscopy (CLSM; LSM 710, Germany) using Live/Dead bacterial viability kit. Briefly, the bacterial culture film was prepared on the sterilised glass plate using bacterial strains (100 μL; 1×10^8 cells/mL) and LB broth media. Then, the prepared hydrogel group was treated with the bacterial bio-filmed plates and incubated for 24 hours as previously mentioned above. After the treatment, the PBS medium was used to eliminate non-adhesion bacterial cells at the surface of glass plates, and stained with acridine orange (0.01%). The survived bacterial cells after treatment were visualised by CLSM microscopic technique at 540 nm emission wavelength.

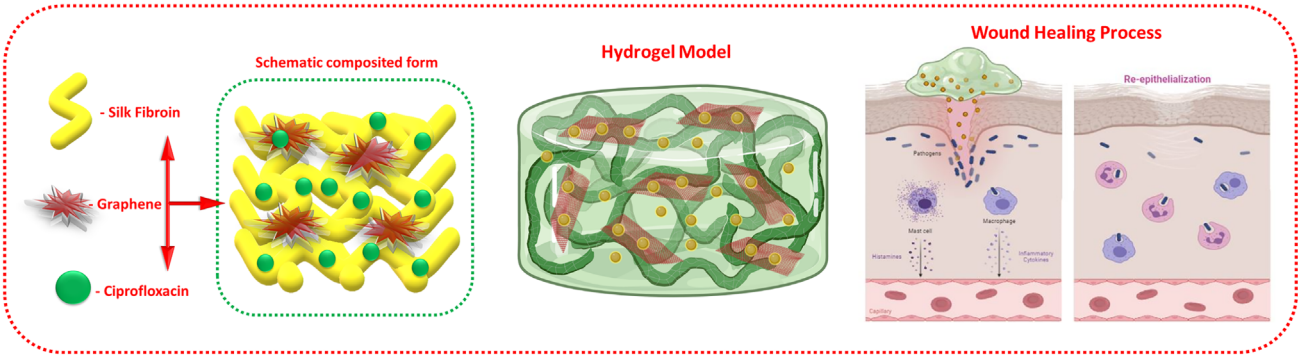

FIGURE 1 Schematic illustration of the present investigation, which is represented as CX and GO-loaded SFP network to the effective wound healing process

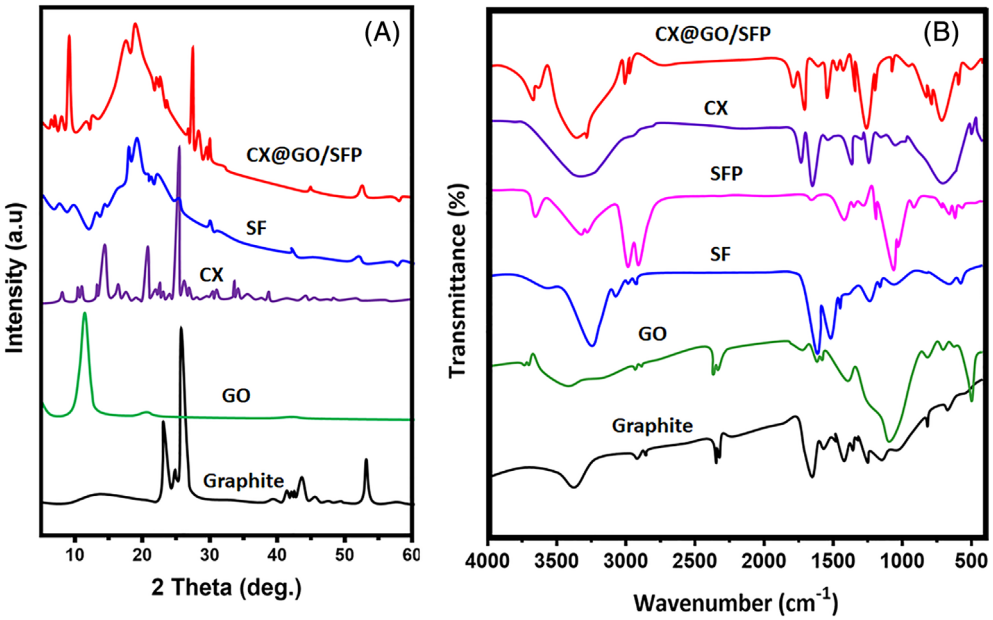

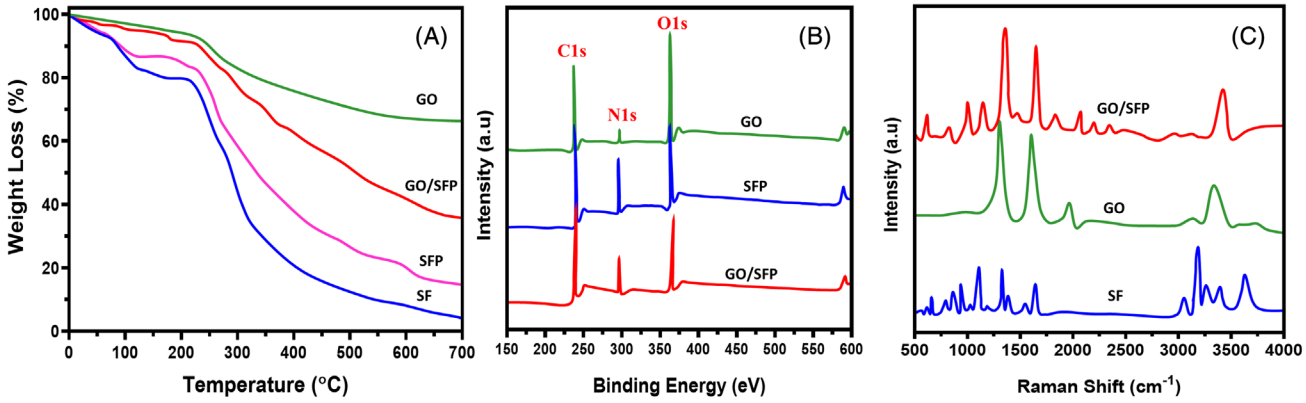

FIGURE 3 Thermal stability, elemental composition and chemical structural behaviours of fabricated hydrogel groups were analysed and presented using TGA (A), XPS (B) and Raman spectroscopic (C) methods

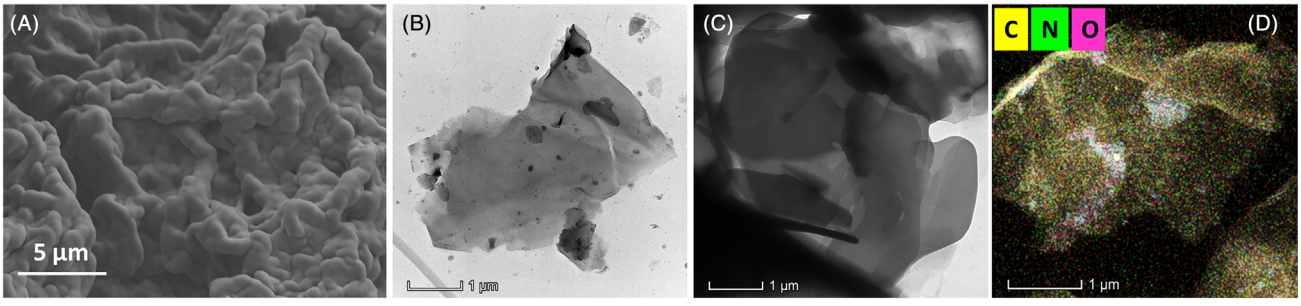

FIGURE 4 Morphological observations by FE-SEM and TEM microscopic techniques: A, FE-SEM image of GO-loaded SFP hydrogel structure, B and C, TEM images of GO and GO/SFP hydrogel groups and EDX mapping (D) analysis of GO/SFP hydrogel

2.7 | In vitro biocompatibility

For cell culture experiment, primarily, the prepared hydrogel groups were saturated in ethanol and followed by PBS medium to become sterilised samples. In the meantime, human fibroblast culture was prepared using fibroblast-based growth media (basal medium (DMEM and antibiotics (1%) and FBS (10%) supplemented with growth factor kit) and dispersed hydrogel samples were added to the culture at suitable humidified incubation

conditions (37°C and 5% CO_2). The cell survival rate was observed by MTT assay at different incubation time intervals and also in vitro wound healing efficiency and proliferation morphology were observed by optical microscopic observation.

2.8 | In vivo wound model

All the animal experimental protocols were performed under approved guidelines and animal care committee of the first people's hospital of Wenling, PR China. For the animal experiments, matured male Sprague-Dawley (SD) rats (240 ± 30 g) were purchased from the experimental animal center and experimental samples were divided into three groups including control, GO/SF and CF@GO/SF hydrogel groups and rats were arbitrarily assigned to each group (n = 6). Firstly, the rats were systematically anaesthetised with chloral hydrate. Then, the burn wounds were created under metal punch heated to 100°C through forcefully pressed on shaved skin site of the rats. The damaged wound site of burn injury was further surgically removed by surgical sander device to attain a deep degree burn injury with required wound depth. Created burn wound sites were covered by SF hydrogel (control) and other developed hydrogel groups. The wound healing efficiency of the treated groups was observed by photograph on days 3, 6, 12 and 18 days of post-injury. The healed wound area percentage was determined by ImagePro6 software and plotted graph by dividing post-operative wound area versus initial wound area. Further, wound healing efficiency of the hydrogel-treated samples was evaluated by histological (H&E stain and MTS stain) examinations on different post-operative days.

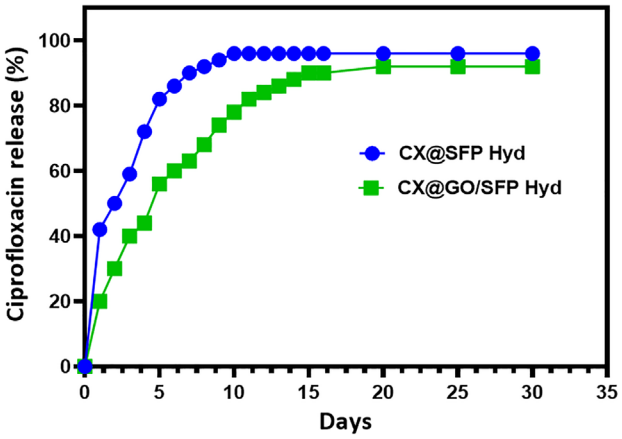

FIGURE 5 In vitro ciprofloxacin drug release potential of fabricated SFP and GO/SFP hydrogel groups under PBS medium in different time intervals

2.9 | Statistical analysis

All the obtained experimental data were stated as standard mean (±) deviation (SD). The statistical analysis

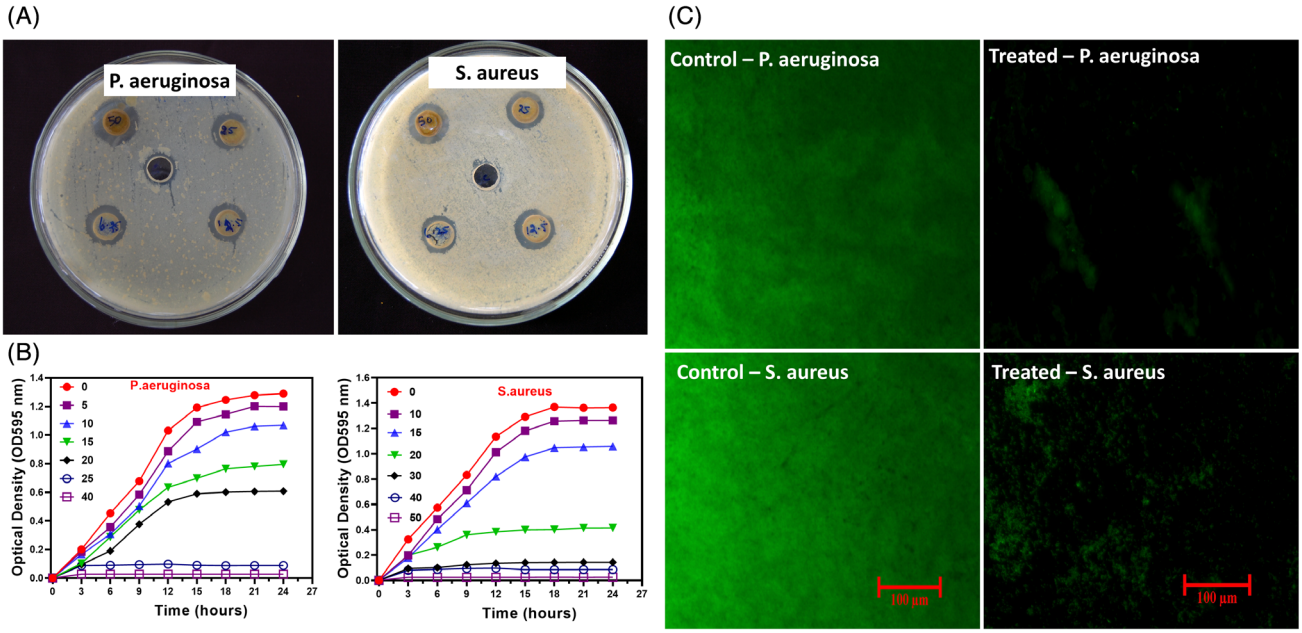

FIGURE 6 In vitro antibacterial analyses: A, Inhibition zone parameters, B, Bacterial growth curve and C, biofilm fluorescence images of the treated with CX@GO/SFP hydrogel group at different concentrations against *P. aeruginosa* and *S. aureus* bacterial pathogens

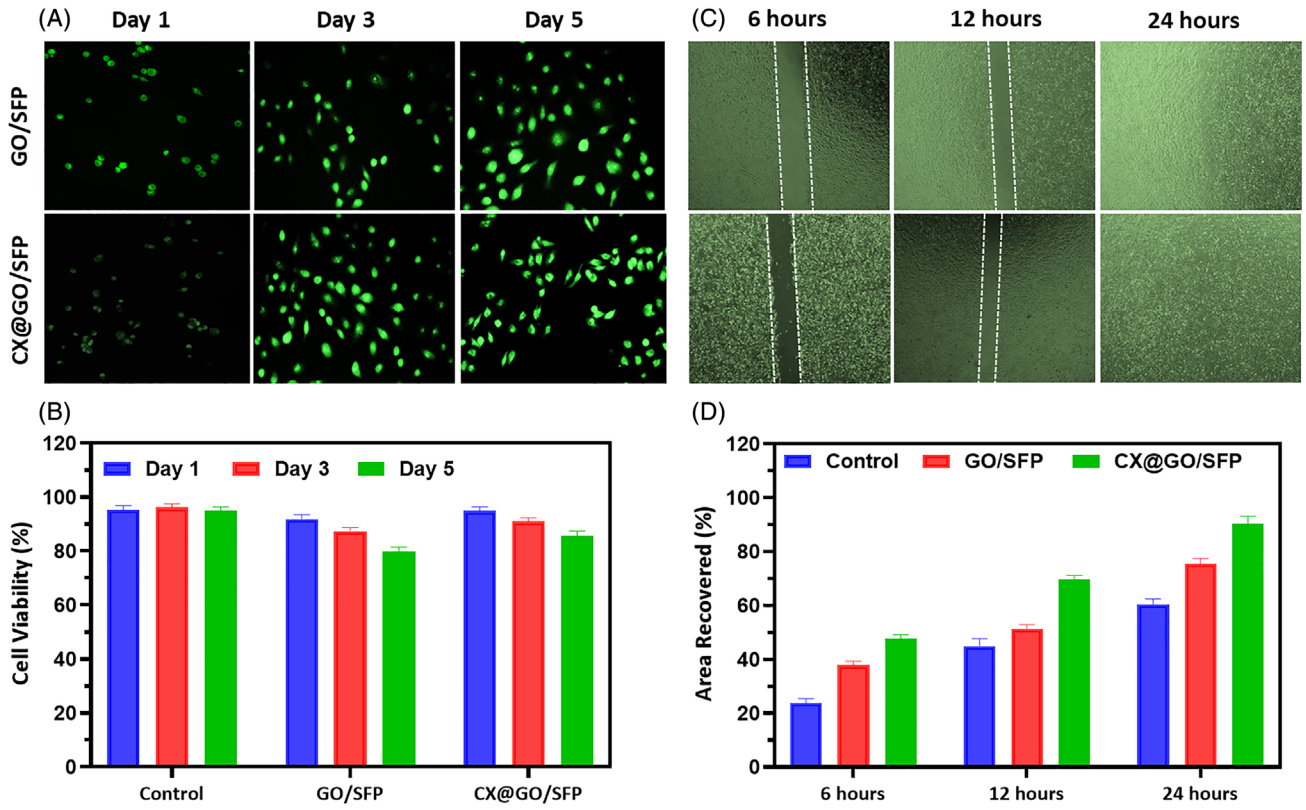

FIGURE 7 In vitro cytocompatibility of the prepared hydrogel groups on the L929 human fibroblast cells; A, epifluorescence microscopic observation of L929 cells treated with GO/SFP and CX@GO/SFP materials at different incubation times (1, 3 and 5 days), B, Quantitative in vitro cell viability rate, C, microscopic observation of wound scratch assay treated with GO/SFP and CX@GO/SFP materials at different incubation time (6, 12 and 24 hours) and D, quantitative analysis of area recovered percentage in the wound scratch assay

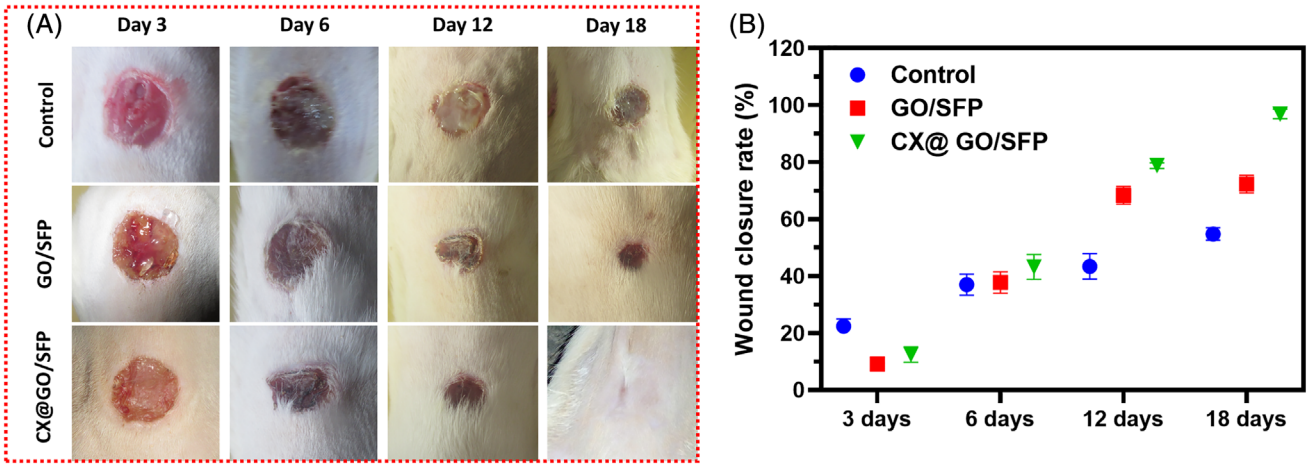

FIGURE 8 In vivo burn wound model treated with the control, GO/SFP and CX@GO/SFP hydrogel groups and photographed (A) on different post-surgery days of 3, 6, 12 and 18 and quantitative measurement of wound closure rate (B), respectively; UL, ulceration; IC, inflammatory cells; IF, inflammatory infiltrates; FB, fibroblast cells; RE, reepithelialisation; DE, dermis layer (magnification ×40)

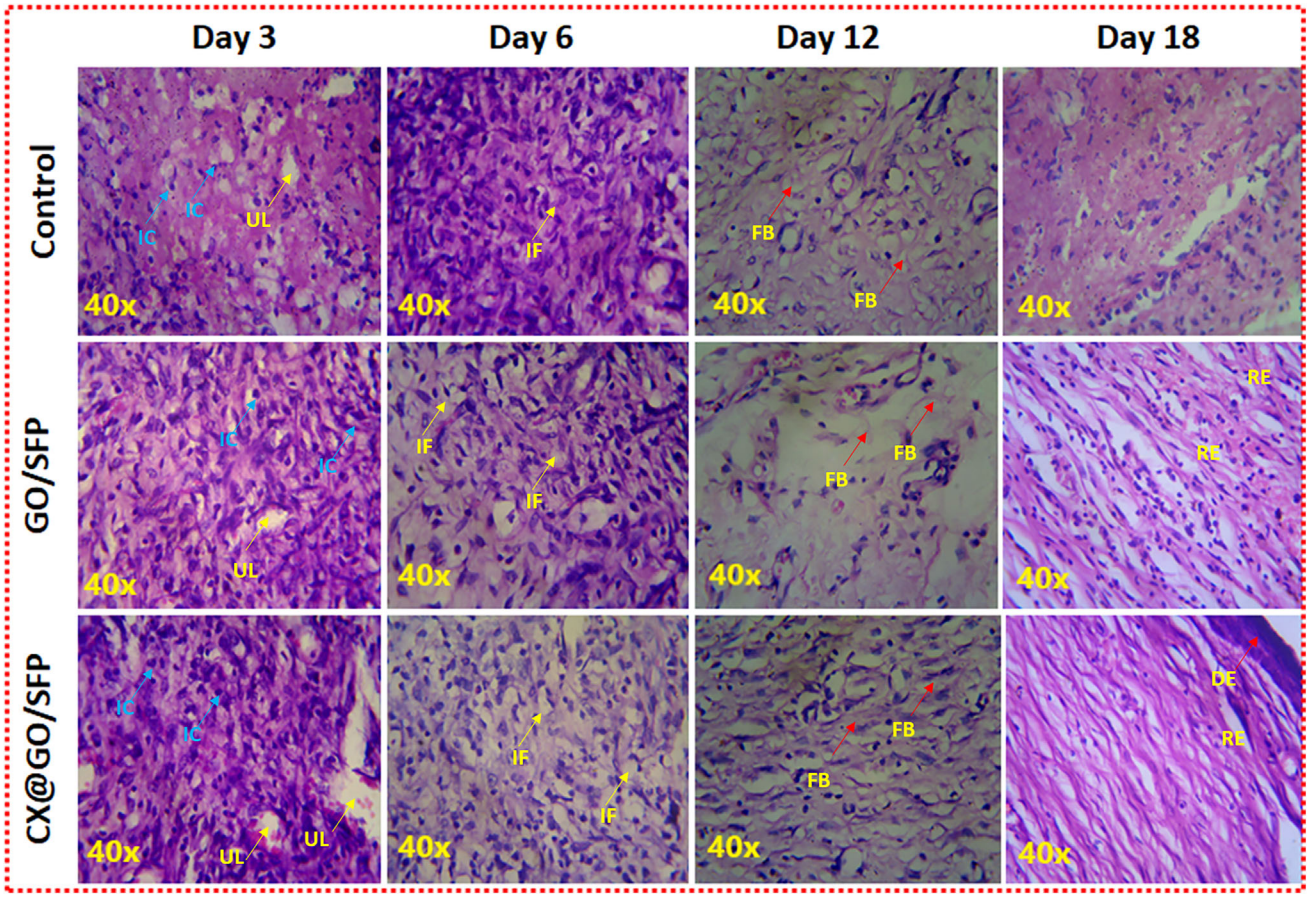

FIGURE 9 Histological observations of harvested in vivo wound specimens using H&E staining at different post-treatment days

was performed by one-way ANOVA analysis and Student's *t*-test software. A value of $P < .05$ was considered statistically significant value.

3 | RESULTS AND DISCUSSION

The present research investigation presented the CX-loaded GO functionalised SFP polymeric network for effective bacterial inhibition and wound healing application as schematically illustrated in Figure 1. The structural interactions and phase purity of the as-prepared graphene oxide and GO-distributed SF hydrogel groups were investigated by XRD and FTIR spectroscopic methods as shown in Figure 2. The XRD pattern results show characteristic peaks and planes of respective crystalline components of GO and Silk (I and II) structures as well as presented in the composited formations. Specifically, sharp peak was observed at $2\Theta = 11.1^{\circ}$ with an interlayer distance of 7.90 Å specify the efficacious formation of GO nanoformulation, which is momentously consistent with the previous reports.[42] In addition, no other peaks of graphite were observed in the respective XRD pattern of GO confirm the completed transformation of GO by the Hummers method.[41] The XRD curve of bare SF protein exhibits the major typical peaks at 25.2°, 20.7° and 9.7°, representing the presence of silk (I and II) structures. After composited hydrogel formation, XRD peaks of CX@GO/SF hydrogel group exhibited chief diffraction peaks at 45.5, 50.2 and 75.3, which demonstrate successful distribution of ciprofloxacin and GO nanostructure in the silk II amorphous polymeric network, which can be confirmed by broad and noise peaks observations. Prominently, XRD curve of CX@GO/SF hydrogel group shows main major and well-defined peaks of crystalline GO and CX molecules with silk II structures, which established that effective uniform distribution of GO nanostructure into the silk structure.[26]

The structural formation and interaction of GO-incorporated SF were verified by FTIR spectral analysis as shown in Figure 2B. Generally, the structure of SF polymer has been composed of important key structural conformational states such as random coil, α-helix and β-sheets, which can be stated as silk I and silk II structures. In the FTIR spectrum, SF structural formations could be established by respective amide IR bands at the

ranges of 1600 to 1700 cm^{-1} (Amide I), 1500 to 1600 cm^{-1} (Amide II) and 1200 to 1350 (Amide III). The spectral data of bare SF polymer without any treatment show absorption peaks at 1660 cm^{-1} (Amide I) and 1546 cm^{-1} (Amide I), attributed to the random coil structure. The band of GO/SF and CX@GO/SF hydrogel groups exhibits well-defined absorption peaks of amide I and amide II shifted to lower wavenumber values to 1626 and 1525 cm^{-1}, respectively, corresponding to the successful silk II structural confirmation, which additionally confirmed transformation state of SF from random coil to β-sheet. Importantly, after incorporation of GO with SF, no significant band shifts were observed at respective amide (I and II) peaks, demonstrating that the distribution of GO nanoformulation does not disturb the conformational states of SF polymer. Meanwhile, the main characteristic absorption peaks of graphene oxide (C═O; 1720 cm^{-1} & C—OH; 1060 cm^{-1}) existed in the spectra of the composited group, which established successful incorporation of GO into the SF hydrogel structure.[43,44]

The materials stability and thermal properties of SF, GO and GO/SFP were determined by the TGA analysis (Figure 3A). Generally, SF and GO nanomaterials are unstable at higher temperatures. Nonetheless, we could confirm thermal stability and presentation of GO nanomaterial through TGA method, which can be an additional proof of GO formation and incorporation. All the prepared groups have primary weight loss at 100°C, which can be corresponded to the elimination of adsorbed water (H_2O) molecules. Another slight mass reduction was observed at 200°C in GO and GO/SF hydrogel group, which may be because of the functional groups decomposition of labile oxygen presented in GO. Importantly, degradation and mass reduction peaks were observed at the temperature range of 270°C to 290°C, demonstrating the existence of silk I and silk II structures and its degradations. The degradation percentage of GO/SF was significantly decreased when compared with the bare SF polymer, demonstrating strong intermolecular interactions between GO and SF polymer molecular structures. The elemental presentations and functional group states were evaluated by XPS spectroscopic analysis as exhibited in Figure 3B. The resulted data demonstrated that the presence of carbon, oxygen and nitrogen atoms and C/O/N ratio of SF, GO and GO-loaded SFP hydrogel groups. Generally, the distribution of GO nanostructure into SF network could induce the new formation of oxygen-containing groups (etc., aldehyde, carboxyl and carbonyl), and additionally providing increasing number of hydrophilic groups in the SF polymeric network.[45,46] Further, surface structure and composition of prepared graphene oxide and structural interactions between GO nanostructure and SF polymeric network were evaluated by Raman spectra as shown in Figure 3C. The observed Raman spectra of GO-incorporated SF hydrogel group exhibited the existence of hybridised (sp^2 and sp^3) form of carbon atom presented in the graphite and prepared GO nanostructure, which was compared with the spectra of bare GO as displayed in Figure 3C (GO). The Raman spectra of bare graphite commonly have two well-defined and intense peaks at a range of 1350 and 1590 cm^{-1}, corresponded to the D-band and G-band, respectively, which would be main peaks to explain about defects and broken symmetry of basal plane and vibrational mode (Eg) of sp^2 hybridised carbon atom of graphitic carbon atom after the transformation reaction of graphite to graphene oxide. Importantly, the spectra of GO and GO-incorporated SFP have slightly shifted bands (G-band and D-band) to higher wavenumbers, which confirmed the transformation of graphene oxide from graphite and also demonstrating uniform distribution in the SF polymeric network. Meanwhile, the main reasons of these shifts are responsible to blue shift of G-band frequencies and chemical doping in GO nanostructure.[47-49]

The smooth morphology of GO and porous morphology of the GO-distributed SF hydrogel groups were observed and visualised by FE-SEM and TEM analyses as exhibited in Figure 4. SEM morphological analysis of GO-incorporated lyophilised SF hydrogel group (Figure 4A) exhibited smooth and homogeneously distributed porous morphology, which indicates that the prepared hydrogel material can be highly suitable for sustained release of antibiotic and healing mechanism in wound regeneration therapy. Meanwhile, uniform distribution of GO nanostructures into the SF network was further confirmed by transmission electron microscopic (TEM) analysis, which established that sheet-like GO nanostructure evenly embedded in the SF matrix without any agglomerations as shown in Figure 4B,C. The microscopic analyses were significantly consistent with the discussed spectroscopic analyses for strong molecular and structural interaction between GO and SF components, because of noteworthy oxygen-containing groups on the GO nanostructure and diverse polar side-chain molecules onto SF polymer. Additionally, EDX mapping analysis (Figure 4D) exhibited the elemental presentation of carbon, oxygen and nitrogen at suitable composition on GO-loaded SFP hydrogel group.

The release kinetics of ciprofloxacin from SFP and GO/SFP hydrogel groups were investigated by in vitro drug release analysis method in PBS buffer (pH = 7.4) as exhibited in Figure 5. The drug release observation from SFP and GO/SFP hydrogel groups demonstrated that the

release of CX was bibasic in nature, and has burst release at initial and followed by sustained release from developed hydrogel groups. Specifically, GO/SFP hydrogel group has more favourable and sustained release profile when compared with the SFP group, because of the effective incorporation of graphene oxide nanostructures that may influence the steady release of CX molecules. The resultant data exhibited GO/SFP hydrogel group has achieved higher drug release rate approximately 98.5 ± 2.5 at 4 days. As stated in previous reports, the probable reason of initial burst release might be a quick solubilisation of surface-attached CX drug molecules at the amorphous SF polymeric network and also have more possibilities of direct contact of PBS media. Then, sustained release could be observed during increase in time because the CX molecules are strongly attached onto the GO crystalline form and also the main cause of controlled degradation behaviour silk protein network.[38,50]

The antibacterial efficacy of the prepared CX-loaded GO/SFP hydrogel groups was evaluated by the methods of inhibition zone, growth curve analysis and biofilm assay methods as shown in Figure 6. The bactericidal activity of the hydrogel groups in the presence and absence of CX was performed and observed by inhibition zone parameters on the Petri dish as shown in Figure 6A. It can be detected that bare SFP hydrogel group did not display any antibacterial activity, meanwhile GO-loaded SFP shows minimum antibacterial activity because of some GO nanostructure release from hydrogel group when treated on the bacterial cell surfaces. By contrast, CX-loaded GO/SFP composite hydrogel group showed broad inhibition zone against clinically approved *P. aeruginosa* and *S. aureus* bacterial pathogens when compared with the other groups, because of burst release of CX from the hydrogel scaffolds and antibacterial potential of the ciprofloxacin. In addition, antibacterial activity of the developed CX-loaded GO/SFP hydrogel was further evaluated by concentration-dependent growth curve and biofilm analysis methods. The observation of growth curve analysis demonstrated that the cytotoxic behaviour of CX@GO/SFP was significantly augmented when increasing concentration from 0 to 40 μg/mL with increasing incubated time. It has been established that CX@GO/SFP hydrogel group has promisingly played against bacterial growth with suitable concentrations compared with other samples as shown in Figure 6B. The biofilm analysis against *P. aeruginosa* and *S. aureus* pathogens treated with CX@GO/SFP also exhibited that effective bactericidal activity and biofilm inhibition when compared with the control group (Figure 6C), which is strongly supported to demonstrate material suitability for the wound healing treatment. The observation of bacterial analyses demonstrated that the developed hydrogel group could greatly help to treat on time and early stage wound infections.[51,52]

As reported previously, the growth and attachment of fibroblast are greatly essential for in vivo wound healing process, hence we have chosen human fibroblast (L929) cells to investigate cytocompatibility of the developed hydrogel groups.[53,54] In the present study, the cell survival and proliferation rate of the prepared material were observed by MTT assay method and optical microscopic analysis on L929 cells (Figure 7). The in vitro scratch wound healing assay method displayed effective cell healing and greater area recovered rate treated of GO/SFP and CX@GO/SFP hydrogel groups with greater cell distribution by visible lamellipodia and elongated morphological structure, which confirmed that the hydrogel groups have suitable cell compatibility and proliferation ability because of its hydrogels hydrophobicity and surface roughness of GO coating (Figure 7A,B). Meanwhile, the prepared hydrogel groups have achieved sophisticated cell survival rate on L929 fibroblast cell with increasing incubation time (1, 3 and 5 days) as displayed in Figure 7C. Furthermore, the reasons of favourable cell survival could be a microenvironment of silk protein, which has been suitable to cell proliferations and attachment on their surface. Generally, higher dose of GO nanostructure may be cytotoxic to cell proliferations and viability because bare GO caused increase in intracellular stress, irrevocably leading to cell death. Nonetheless, the present observation of cell compatibility outcome confirmed the optimised GO distributions into SF for favourable wound dressing treatment.[55-57]

On the basis of favourable outcomes from above observations, the in vivo wound healing efficiency of fabricated hydrogel groups was investigated and shown in Figures 8 and 9. Generally, developed wound dressing materials should be influenced by four different stages of in vivo wound healing mechanisms including inflammation, reformation of granulation tissue, new tissue remodelling and reepithelialisation.[4,16] In the burn wound healing therapy, tangential excision method is the most common and routinely applied treatment after burn injury of deep-partial thickness burn; meanwhile, severe side effects have occurred including heavy bleeding, surgical stress and importantly subtraction of extra normal tissues. Hence, it is necessary to find a potential and multifunctional wound dressing material with abilities to maintain moist microenvironment, protection from microbial infections and eradicating dead cells and provide effective wound healing. In the present investigation, different hydrogel dressings were systematically

covered on the deep-partial thickness burn site. The representative macroscopic burn wound treatment images were displayed for negative control (bare wound), positive control (Mepitel®), GO/SFP and CX@GO/SFP hydrogel dressing on days 3, 6, 12 and 18 as shown in Figure 8A. The results presented that hydrogel dressing embedded burn wounds have superior autolytic debridement similar to the positive control, which is significant to primary healing process in burn wound closure. As shown in Figure 8B, wound closure rate of CX@GO/SFP hydrogel promisingly enhanced with increasing post-injury days when compared with the GO/SFP group. Interestingly, the developed CX@GO/SFP hydrogel group has better healing performance than standard positive control, which demonstrated that the outcomes of the fabricated material could be an effective source for future generation burn wound healing treatment.

In vivo therapeutic potential of prepared wound dressing was further confirmed through histological (H&E staining) observations using harvested skin specimens on days 3, 6, 12 and 18 as shown in Figure 9. The pathological images showed surface ulceration and damaged partial thickness dermis at day 3—a deep-partial thickness of burn injury was demonstrated. At day 6, dermal tissue and more inflammatory cells were found at negative control group when compared with the other groups and specifically reduced eschar tissues were displayed in GO/SFP and CX@GO/SFP hydrogel groups, which are similar to the positive control. The greater number of fibroblast cells presence and greater reepithelialisation formation were observed for hydrogel groups when compared with the control at day 12, which demonstrated that it could be greatly helpful to wound regeneration.[58,59] The histological observation at day 18 obviously evidenced to completed wound reformation with epidermal layer. The results of H&E staining observation clearly demonstrated that the developed CX@GO/SFP hydrogel could significantly reduce initial stage necrotic tissue denaturation, favourable inflammatory response, increased fibroblast formation, quicken the reepithelialisation and improve the eminence of wound regeneration.

4 | CONCLUSION

In the present research investigation, novel combined CX-loaded GO/SFP hydrogel dressing was successfully fabricated and systematically established for their antibacterial and wound regeneration potential after burn injury. The chemical and mechanical analyses demonstrated the intermolecular interactions and modulated mechanical strength of GO-distributed SFP network for the advantages of wound dressing. In vitro antibacterial observations established the CX-loaded hydrogel group has effective bactericidal action against clinically approved wound infectious pathogens, which could lead to a major role in the burn wound treatment. Importantly, hydrogel dressings have promisingly achieved cytocompatibility with L929 fibroblast cells with enhanced cell survival and proliferation rate. The composite hydrogel dressing with CX drug molecules significantly enhanced the in vivo wound regeneration ability, which was evident through reduced inflammatory response, effective fibroblast formation and reepithelialisation for the hydrogel-treated burn wound models. Therefore, GO-incorporated SFP hydrogel can be used as a promising dressing material to promote wound regeneration in burn injury treatment.

ACKNOWLEDGEMENTS

The Authors wholeheartedly acknowledge Heilongjiang Youth Science Foundation (QC2016101), Harbin Science and Technology Innovation Talents Research Foundation (2016 RAQXJ159, 2016 RAXYJ069), Heilongjiang Provincial Health and Family Planning Commission Research Project (2018-082).

ORCID

Linlu Chen https://orcid.org/0000-0003-0115-6712

REFERENCES

1. Pan Z, Ye H, Wu D. Recent advances on polymeric hydrogels as wound dressings recent advances on polymeric hydrogels as wound dressings. *APL Bioeng*. 2021;5(1):1-16. https://doi.org/10.1063/5.0038364.
2. Saghazadeh S, Rinoldi C, Schot M, et al. Drug delivery systems and materials for wound healing applications. *HHS Public Access*. 2018;127:138-166. https://doi.org/10.1016/j.addr.2018.04.008.
3. Gupta P, Chhibber S, Harjai K. Efficacy of purified lactonase and ciprofloxacin in preventing systemic spread of Pseudomonas aeruginosa in murine burn wound model. *Burns*. 2015;41(1):153-162. https://doi.org/10.1016/j.burns.2014.06.009
4. Madaghiele M, Demitri C, Sannino A, Ambrosio L. Polymeric hydrogels for burn wound care: advanced skin wound dressings and regenerative templates. *Burns Trauma*. 2014;2(4):153-161.
5. Li Z, Zhou F, Li Z, et al. Hydrogel cross-linked with dynamic covalent bonding and micellization for promoting burn wound healing. *ACS Appl Mater Interfaces*. 2018;10(30):25194-25202. https://doi.org/10.1021/acsami.8b08165. Epub 2018 Jul 23.
6. Guo X, Liu Y, Bera H, et al. α-Lactalbumin-based Nano fiber dressings improve burn wound healing and reduce scarring. *ACS Appl Mater Interfaces*. 2020;12(41):45702-45713. https://doi.org/10.1021/acsami.0c05175.
7. Mai B, Jia M, Liu S, et al. Smart hydrogel-based DVDMS/bFGF nanohybrids for antibacterial phototherapy with multiple damaging sites and accelerated wound healing. *ACS Appl Mater Interfaces*. 2020.

8. Op RC, Walboomers XF, Jansen JA, Wagener FADTG. Design considerations for hydrogel wound dressings: strategic and molecular advances. *Tissue Eng B: Rev*. 2020;26(3):230-248.
9. Tavakoli S, Klar AS. Advanced hydrogels as wound dressings. *Biomolecules*. 2020;10:1169-1189. https://doi.org/10.3390/biom10081169.
10. Lopez N. Hydrogel dressings and their application in burn wound care; 2012.
11. Raveendran NT, Mohandas A, Ramachandran R, Menon AS, Biswas R, Jayakumar R. Ciprofloxacin and fluconazole containing fibrin nanoparticles incorporated chitosan bandages for the treatment of Polymicrobial wound infections ciprofloxacin and fluconazole containing fibrin nanoparticles incorporated chitosan bandages for the treatment. *ACS Appl Bio Mater*. 2019;2(1):243-254. https://doi.org/10.1021/acsabm.8b00585.
12. Nasiri R, Arsalani N, Panahian Y. One-pot synthesis of novel magnetic three-dimensional graphene/chitosan/nickel ferrite nanocomposite for lead ions removal from aqueous solution: RSM modelling design one-pot synthesis of novel magnetic three-dimensional graphene/chitosan/nickel. *J Clean Prod*. 2018;201 (August):507-515. https://doi.org/10.1016/j.jclepro.2018.08.059
13. Huang W, Wang Y, Huang Z, et al. On-demand dissolvable self-healing hydrogel based on carboxymethyl Chitosan and cellulose nanocrystal for deep partial thickness burn wound healing. *ACS Appl Mater Interfaces*. 2018;10(48):41076-41088. https://doi.org/10.1021/acsami.8b14526.
14. Choudhary P, Ramalingam B, Das SK. Fabrication of Chitosan-reinforced multifunctional graphene nanocomposite as antibacterial Scaffolds for hemorrhage control and wound-healing application. *ACS Biomater Sci Eng*. 2020;6(10):5911-5929. https://doi.org/10.1021/acsbiomaterials.0c00923.
15. Wang Q, Chu Y, He J, et al. A graded graphene oxide-hydroxyapatite/silk fibroin biomimetic scaffold for bone tissue engineering. *Mater Sci Eng C*. 2017;80:232-242. https://doi.org/10.1016/j.msec.2017.05.133
16. Uzun M. A review of wound management materials. *J Textile Eng Fashion Technol*. 2018;4(1):53-59.
17. Balu R, Reeder S, Knott R, et al. Tough Photocrosslinked silk fibroin/graphene oxide nanocomposite hydrogels. *Langmuir*. 2018;34(31):9238-9251.
18. Fan L, Yi J, Tong J, et al. Preparation and characterization of oxidized Konjac Glucomannan/Carboxymethyl chitosan/graphene oxide hydrogel. *Int J Biol Macromol*. 2016;91:358-367. https://doi.org/10.1016/j.ijbiomac.2016.05.042
19. Wang Z, Yang H, Li Y, Zheng X. Robust silk fibroin/graphene oxide aerogel fiber for radiative heating textiles. *ACS Appl Mater Interfaces*. 2020;12(13):15726-15736. https://doi.org/10.1021/acsami.0c01330.
20. Wang K, Wang S, Ma Q, Wang K, Ma P. Strong and biocompatible three-dimensional porous silk fibroin/graphene oxide scaffold prepared by phase separation. *Int J Biol Macromol*. 2018;111:237-246. https://doi.org/10.1016/j.ijbiomac.2018.01.021.
21. Selvaraj S, Fathima NN. Fenugreek incorporated silk fibroin nanofibers: a potential antioxidant scaffold for enhanced wound healing. *ACS Appl Mater Interfaces*. 2017;9(7):5916-5926. https://doi.org/10.1021/acsami.6b16306.
22. Wang J, Chen Y, Zhou G, Chen Y, Mao C, Yang M. Polydopamine-coated *Antheraea pernyi* (*A. pernyi*) silk fibroin films promote cell adhesion and wound healing in skin tissue repair. *ACS Appl Mater Interfaces*. 2019;11(38):34736-34743. https://doi.org/10.1021/acsami.9b12643.
23. Zhou W, Jia Z, Xiong P, et al. Bioinspired and biomimetic AgNPs/gentamicin-embedded silk fibroin coatings for robust antibacterial and osteogenetic applications. *ACS Appl Mater Interfaces*. 2017;9(31):25830-25846. https://doi.org/10.1021/acsami.7b06757.
24. Zeng D, Cao L. Enhanced bone regeneration of the silk fibroin electrospun scaffolds through the modification of the graphene oxide functionalized by BMP-2 peptide. *Int J Nanomed*. 2019;14:733-751. https://doi.org/10.2147/IJN.S187664.
25. Zhang C, Zhang Y, Shao H, Hu X. Hybrid silk fibers dry-spun from regenerated silk fibroin/graphene oxide aqueous solutions. *ACS Appl Mater Interfaces*. 2016;8(5):3349-3358.
26. Wang L, Lu C, Zhang B, Zhao B. Fabrication and characterization of flexible silk fibroin films reinforced RSC advances fabrication and characterization of flexible silk fi broin films reinforced with graphene oxide for biomedical applications. *RSC Adv*. 2014;4:40312-40320. https://doi.org/10.1039/C4RA04529G
27. Wang S, Ma Q, Wang K, Chen H. Improving antibacterial activity and biocompatibility of bioinspired electrospinning silk fibroin nanofibers modified by graphene oxide. *ACS Omega*. 2018;3(1):406-413. https://doi.org/10.1021/acsomega.7b01210.
28. Shao W, He J, Sang F, et al. Enhanced bone formation in electrospun poly(l-lactic-co-glycolic acid)-tussah silk fibroin ultrafine nanofiber scaffolds incorporated with graphene oxide. *Mater Sci Eng C*. 2016;62:823-834. https://doi.org/10.1016/j.msec.2016.01.078
29. Wang SD, Ma Q, Wang K, Chen HW. Improving antibacterial activity and biocompatibility of bioinspired electrospinning silk fibroin nanofibers modified by graphene oxide. *ACS Omega*. 2017;3(1):406-413.
30. Liu Z, Shang S, Chiu K, Jiang S, Dai F. Fabrication of silk fibroin/poly(lactic-co-glycolic acid)/graphene oxide microfiber mat via electrospinning for protective fabric. *Mater Sci Eng C*. 2020;107:110308-110316. https://doi.org/10.1016/j.msec.2019.110308
31. Li M, Xiong P, Mo M, Cheng Y, Zheng Y. Electrophoretic-deposited novel ternary silk fibroin/graphene oxide/hydroxyapatite nanocomposite coatings on titanium substrate for orthopedic applications. *Front Mater Sci*. 2016;10(3):270-280.
32. Shi M, Zhang H, Song T, et al. Sustainable dual release of antibiotic and growth factor from pH-responsive uniform alginate composite microparticles to enhance wound healing. *ACS Appl Mater Interfaces*. 2019;11:22730-22744.
33. Heal CF, van Driel ML, Lepper PD, Banks JL. Topical antibiotics for preventing surgical site infection in wounds healing by primary intention. *Cochrane Database Syst Rev*. 2014;11(11).CD011426-CD011430. https://doi.org/10.1002/14651858.CD011426.
34. Feng X, Zhang Z, Li X, et al. Mutations in gyrB play an important role in ciprofloxacin-resistant *Pseudomonas aeruginosa*. *Infect Drug Resist*. 2019;12:261-272.
35. Nelson JD, Silverman V, Lima PH, Beckman G. Corneal epithelial wound healing: a tissue culture assay on the effect of antibiotics. *Curr Eye Res*. 1990;9(3):277-285.
36. Zhang M, Jiang Z, Li D, et al. Oral antibiotic treatment induces skin microbiota Dysbiosis and influences wound healing. *Microb Ecol*. 2015;69(2):415-421.
37. Roy DC, Tomblyn S, Isaac KM, et al. Ciprofloxacin-loaded keratin hydrogels reduce infection and support healing in a

porcine partial-thickness thermal burn. *Wound Repair Regener*. 2016;24(4):657-668. https://doi.org/10.1111/wrr.12449.

38. García MC, Aldana AA, Tártara LI, et al. Bioadhesive and biocompatible films as wound dressing materials based on a novel dendronized chitosan loaded with ciprofloxacin. *Carbohydr Polym*. 2017;175:75-86. https://doi.org/10.1016/j.carbpol.2017.07.053
39. Zhang H, Zhao J, Xing T, Lu S. Fabrication of Silk Fibroin/Graphene Film with High Electrical Conductivity and Humidity Sensitivity. *Polymers*. 2019;11(11):1774-1786. https://doi.org/10.3390/polym11111774.
40. Jing J, Liang S, Yan Y, Tian X, Li X. Fabrication of hybrid hydrogels from silk fibroin and tannic acid with enhanced gelation and antibacterial activities. *ACS Biomater Sci Eng*. 2019;5(9):4601-4611.
41. Cao N, Zhang Y. Study of reduced graphene oxide preparation by Hummers' method and related characterization. *J Nanomater*. 2015;2015:1-5.
42. Chen D, Li L. Environment-friendly preparation of reduced graphene oxide nanosheets via amino acid. *Nanotechnology*. 2011;22:325601-325608. https://doi.org/10.1088/0957-4484/22/32/325601.
43. Altinbasak I, Jijie R, Barras A, et al. Reduced graphene oxide embedded polymeric nanofiber mats: an 'on-demand' photothermally-triggered antibiotic release platform. *ACS Appl Mater Interfaces*. 2018;10(48):41098-41106. https://doi.org/10.1021/acsami.8b14784.
44. Wang W, Liu Y, Yang C, et al. Delivery of Salvianolic acid B for efficient osteogenesis and angiogenesis from silk fibroin combined with graphene oxide. *ACS Biomater Sci Eng*. 2020;6(6):3539-3549.
45. Eivazzadeh-Keihan R, Khalili F, Aliabadi HAM, et al. Alginate hydrogel-polyvinyl alcohol/silk fibroin/magnesium hydroxide nanorods: a novel scaffold with biological and antibacterial activity and improved mechanical properties. *Int J Biol Macromol*. 2020;162:1959-1971. https://doi.org/10.1016/j.ijbiomac.2020.08.090
46. Zhou C, Liu S, Li J, et al. Collagen functionalized with graphene oxide enhanced biomimetic mineralization and in situ bone defect repair. *ACS Appl Mater Interfaces*. 2018;10(50):44080-44091.
47. Kaniyoor A, Sundara R. A Raman spectroscopic investigation of graphite oxide derived graphene. *Aip Adv*. 2012;2:032183-032197.
48. Luo J, Zhang X, Ong'achwa MacHuki J, et al. Three-dimensionally N-doped graphene-hydroxyapatite/agarose as an Osteoinductive scaffold for enhancing bone regeneration. *ACS Appl Bio Mater*. 2019;2(1):299-310.
49. Kaur R, Tabish TA, Trakoolwilaiwan T, et al. Journal of colloid and Interface science microstructure and antibacterial efficacy of graphene oxide nanocomposite fibres. *J Colloid Interface Sci*. 2020;571:239-252. https://doi.org/10.1016/j.jcis.2020.03.037
50. Shanaghi A, Mehrjou B, Ahmadian Z, Reza A, Chu PK. Enhanced corrosion resistance, antibacterial properties, and biocompatibility by hierarchical hydroxyapatite/ciprofloxacin-calcium phosphate coating on nitrided NiTi alloy. *Mater Sci Eng C*. 2021;118(June 2020):111524. https://doi.org/10.1016/j.msec.2020.111524
51. Chen B, Wang J. Antimicrobial hydrogels: promising materials for medical application. *Int J Nanomed*. 2018;12(12):2217-2263. https://doi.org/10.2147/IJN.S154748.
52. Ajmal G, Vasant G, Mittal P, Khan G, Kumar V. Biomimetic PCL-gelatin based nanofibers loaded with ciprofloxacin hydrochloride and quercetin: a potential antibacterial and antioxidant dressing material for accelerated healing of a full thickness wound. *Int J Pharm*. 2019;567(May):118480. https://doi.org/10.1016/j.ijpharm.2019.118480
53. Pasaribu SP, Ginting M, Masmur I, Kaban J, Hestina. Silver chloride nanoparticles embedded in self-healing hydrogels with biocompatible and antibacterial properties. *J Mol Liq*. 2020;310:113263. https://doi.org/10.1016/j.molliq.2020.113263
54. Nair S, Remya NS, Remya S, Nair PD. A biodegradable in situ injectable hydrogel based on chitosan and oxidized hyaluronic acid for tissue engineering applications. *Carbohydr Polym*. 2011;85(4):838-844. https://doi.org/10.1016/j.carbpol.2011.04.004
55. Huang H, Qi X, Chen Y, Wu Z. Thermo-sensitive hydrogels for delivering biotherapeutic molecules: a review. *Saudi Pharm J*. 2019;27(7):990-999. https://doi.org/10.1016/j.jsps.2019.08.001
56. Ishihara K, Oda H, Konno T. Spontaneously and reversibly forming phospholipid polymer hydrogels as a matrix for cell engineering. *Biomaterials*. 2020;230:119628.
57. Bian D, Deng J, Li N, et al. In vitro and in vivo studies on biomedical magnesium low-alloying with elements gadolinium and zinc for orthopedic implant applications. *ACS Appl Mater Interfaces*. 2018;10(5):4394-4408.
58. Beyranvand S, Pourghobadi Z, Sattari S, Soleymani K, Nayebzadeh H, Adeli M. Boronic acid functionalized graphene platforms for diabetic wound healing. *Carbon N Y*. 2019;158:327-336. https://doi.org/10.1016/j.carbon.2019.10.077
59. Liu H, Yuan M, Sonamuthu J, et al. A dopamine-functionalized aqueous-based silk protein hydrogel bioadhesive for biomedical wound closure. *New J Chem*. 2020;44(3):884-891.

How to cite this article: Dong M, Mao Y, Zhao Z, et al. Novel fabrication of antibiotic containing multifunctional silk fibroin injectable hydrogel dressing to enhance bactericidal action and wound healing efficiency on burn wound: In vitro and in vivo evaluations. *Int Wound J*. 2022;19(3):679-691. https://doi.org/10.1111/iwj.13665